Spatial distribution of wave overtopping water behind coastal structures

Spatial distribution of wave overtopping water behind coastal structures

Zhong Peng, Qing-Ping Zou *

Centre for Coastal Dynamics and Engineering, School of Marine Science and Engineering, University of Plymouth, UK

A B S T R A C T

Spatial distribution of random wave overtopping water behind coastal structures was investigated using a numerical model based on Reynolds-Averaged Navier-Stokes solver (RANS) and Volume of Fluid (VOF) surface capturing scheme (RANS-VOF). The computed spatial distributions of wave overtopping water behind the structure agree well with the measurements by Pullen et al (2008) for a vertical wall and Lykke Andersen and Burcharth (2006) for a 1:2 sea dike. A semi-analytical model was derived to relate spatial distribution of wave overtopping water behind coastal structures to landward ground level, velocity and layer thickness on the crest. This semi-analytical model agrees reasonably well with both numerical model results and measurements close to coastal structures. Our numerical model results suggest that the proportion of wave overtopping water passing a landward location increases with a seaward slope when it is less than 1:3 and decreases with a seaward slope when it gets steeper. The proportion of wave overtopping water passing a landward location increases with landward ground level and overtopping discharge. It also increases with the product of incident wave height and wavelength, but decreases with increasing relative structure freeboard and crest width. We also found that the extent of hazard area due to wave overtopping is significantly reduced by using a permeable structure crown. Findings in this study will enable engineers to establish the extent of hazard zones due to wave overtopping behind coastal structures.

1. Introduction

Landward spatial distribution of overtopping water determines the risk of damages and sets restrictions on the use of areas behind the coastal defences. It ultimately affects the placement of roads, walkways, railways, buildings and other infrastructure near a coastal structure. In the UK, the safety issue of developed coasts is of particular concern. Evidence of damages to properties behind coastal structures due to wave overtopping, was most graphically given by the trainload of pig iron washed off Dover East Breakwater in the 1940s and by the destruction of seafront shelters at Sidmouth in 1992 (Allsop et al., 2005).

The complexity of wave interaction with coastal structures has led a great majority of investigators to resort to laboratory experiments and field measurements. For example, a database on wave overtopping consisting of more than 10,000 irregular wave overtopping tests collecting from more than 160 independent projects or test series was established in the EU project CLASH by van der Meer et al. (2009). Recent studies were carried out to investigate the influence of wave obliquity and directional spreading on wave overtopping of rubble mound breakwaters by Lykke Andersen and Burcharth (2009) and combined wave overtopping and storm surge overflow of a levee with a trapezoidal cross section by Hughes and Nadal (2009). Numerical modelling of wave overtopping has gained popularity recently due to increasing computer power. Hu et al. (2000) used the non-linear shallow water equations to study wave overtopping. Liu et al. (1999) introduced a numerical model based on Reynolds-Averaged Navier-Stokes solver (RANS) and Volume of Fluid (VOF) surface capturing scheme (RANS-VOF), developed by Lin and Liu (1998), to study wave overtopping over a caisson breakwater with a porous armour layer. This model was later employed to simulate wave overtopping over rubble mound breakwaters by Losada et al. (2008), over a smooth impermeable seawall by Reeve et al. (2008) and over a levee by Xiao et al. (2009). Different from these authors, Shao et al. (2006) employed a smoothed particle hydrodynamics (SPH) method to investigate wave overtopping over an impermeable sloping seawall. Previous studies on wave overtopping, however, have mainly focused on the overtopping discharge (Owen, 1980; Troch et al., 2004; Schüttrumpf and Oumeraci, 2005; Bruce et al., 2009; van der Meer et al., 2009), there is little work on the spatial distribution of wave overtopping water after a sea defence.

Jensen and Sorensen (1979) measured the spatial distribution of wave overtopping discharges behind a vertical wall in the laboratory and proposed an empirical formula to fit these data. Bruce et al. (2005) and Pullen et al. (2008) carried out field and laboratory experiments of the spatial distribution of overtopping water over a seawall. They established a relationship between the proportion of wave overtopping

* Corresponding author. Tel.: +44 1752586158; fax: +44 1752 586101.
E-mail address: qingping.zou@plymouth.ac.uk (Q.-P. Zou).

water and the distance behind the seawall. Their work focused on the vertical seawall in Samphire Hoe and only considered the spatial distribution of overtopping water at a particular landward ground level. Based on the large and small scale experiments on rubble mound breakwaters, Lykke Andersen and Burcharth (2006) and Lykke Andersen et al. (2007) proposed a formula to relate the landward spatial distribution of the overtopping water to wave steepness, incident angle, significant wave height and landward ground level. EurOtop Manual (EurOtop, 2008) recommended a formula slightly different from that in Lykke Andersen and Burcharth (2006) to predict the landward spatial distribution of overtopping water. This formula is only valid for rubble mound structures with a slope of approximately 1:2 and for angles of wave attack between 0 and 45°.

The spatial distribution of overtopping water has been investigated only in these experiments with relatively low spatial resolution, limited geometries and wave conditions. On the other hand, a numerical model provides an alternative means to give high spatial and temporal resolution information of physical variables in this problem which are difficult to measure in the laboratory or field sites. Numerical models, however, have not been employed to investigate this problem.

The aim of this study is to use RANS-VOF model and introduce a semi-analytical model to investigate the spatial distributions of wave overtopping water behind costal structures, with special attention to the role of wave conditions, structure geometries, and landward ground level in this problem. The predicted landward distributions of wave overtopping water are validated against the measurements by Pullen et al (2008) for a vertical seawall and Lykke Andersen and Burcharth (2006) for a 1:2 dike.

2. Numerical models

RANS-VOF model by Lin and Liu (1998) solves the 2D Reynolds Averaged Navier–Stokes equations by decomposing the instantaneous velocity and pressure fields into the mean and turbulent components. Reynolds stresses were described by an algebraic non-linear k–ε turbulence model. A Volume of Fluid (VOF) method developed by Hirt and Nichols (1981) was employed to capture free surface. Recently, the RANS-VOF model was used widely to simulate wave–structure interaction (Garcia et al., 2004; Lara et al., 2006; Losada et al., 2008; Reeve et al., 2008). This model will be validated by the case of wave overtopping over a smooth impermeable dike with a 1:6 seaward slope (Li et al., 2004; Shao et al., 2006; Li et al., 2007; Ingram et al., 2009).

2.1. Model setup

Fig. 1 shows the setup of numerical simulations. The computation domain is 13.0 m × 1.0 m. The geometry of the sea dike includes a seaward slope of 1:6, a crest with a width of 0.3 m and a height of 0.8 m. An internal wave-maker developed by Lin and Liu (1999) was used to generate regular and irregular waves. A radiation boundary, composed of an open boundary and a sponge layer, was specified at the inlet boundary, and a free-slip boundary condition was applied to the solid boundaries. A zero-stress condition was applied at the free surface and a log-law distribution of mean tangential velocity was applied in the turbulent boundary layer. Turbulent kinetic energy k and dissipation rate ε had zero gradient at the free surface and were assumed to be a function of distance from the boundary and the mean tangential velocity outside of the viscous sublayer (Rodi, 1993; Lin and Liu, 1998). In RANS-VOF model, for turbulent flow the roughness was used to justify whether the surface is hydraulically smooth or rough. Flow was defined as hydraulically rough for roughness $\gamma_f > 10^{-5}$, and the roughness was then used to calculate the friction velocity in the boundary layer. In this study, surface of impermeable structure is assumed as hydraulically smooth, while the surface of permeable structure is assumed as hydraulically rough. The initial condition consists of a still water situation with no current and wave

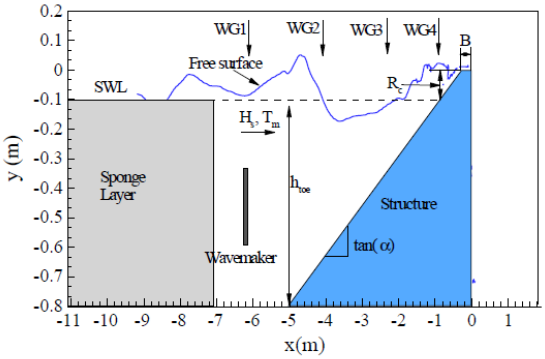

Fig. 1. Sketch of computational domain. WG1 to WG4 represent the locations of four wave gauges in the experiments; h_{toe} is water depth at the toe of structures; SWL is still water level; R_c, B and tan(α) are the structure freeboard, crest width and seaward slope respectively. The origin of coordinates is at the landward end of structure crest with x for horizontal axis and y for vertical axis.

motion. $h_{toe} = 0.7$ m is water depth at the toe of structures; R_c is the structure freeboard; B is structure crest width; tan(α) is the structure slope; WG1 to WG4 are surface elevation gauges in the experiments. Our results show that averaged overtopping discharge of random waves becomes unchanged after 200 s. This was found by Reeve et al. (2008) as well. Therefore simulations limited to 300 s will be used to represent wave overtopping processes to save computational time.

2.2. Surface elevation

The experiment of wave overtopping over a smooth impermeable dike with a 1:6 seaward slope described by Li et al. (2007) was used to validate the RANS-VOF model. Regular waves with a wave height $H = 0.16$ m and wave period $T = 2.0$ s was generated by an internal wave-maker, placed at $x = -6.1$ m with a water depth at the toe of structures of 0.7 m (Fig. 1). Three meshes were used: finest mesh 700 × 100 (0.01 m × 0.01 m), fine mesh 500 × 65 (0.02 m × 0.01 m) and coarse mesh 230 × 32 (0.04 m × 0.02 m). It was found that fine mesh 500 × 65 was fine enough to capture the most important phenomena, thus, fine mesh 500 × 65 was employed in this study. Fig. 2 shows that time history of computed surface elevation at WG2 and WG4 is in good agreement with measurements of Li et al. (2007). The small discrepancy at WG4 may be due to the 3-D effect of highly nonlinear waves at WG4 (Li et al., 2007), characterised by a gradual peaking of crests, flattening of troughs and pitching forward to the sea dike.

2.3. Overtopping discharge

The significant wave height and mean period at the seaward toe of structure, the landward ground level, structure freeboard, structure crest width and structure slope, the layer thickness and velocity on the structure crest are found to be important in wave overtopping process (Schüttrumpf and Oumeraci, 2005; Lykke Andersen and Burcharth, 2006; van der Meer et al., 2009). A definition sketch for overtopping calculations using RANS-VOF model is given in Fig. 3. The origin of coordinates is at the landward end of structure crest with x for horizontal coordinate and y for vertical coordinate; H_s and T_m are the significant wave height and mean period at the seaward toe of structures; R_c, B and tan(α) are the structure freeboard, crest width and slope respectively. $u_{i,j}$, $v_{i,j}$, $\Delta x_{i,j}$, $\Delta y_{i,j}$ are the horizontal velocity, vertical velocity, cell width and cell height in the cell (i, j) respectively. $u_{A,50\%}$ is the wave velocity at the crest of the structure, exceeded by 50% of the incoming waves; h_A is

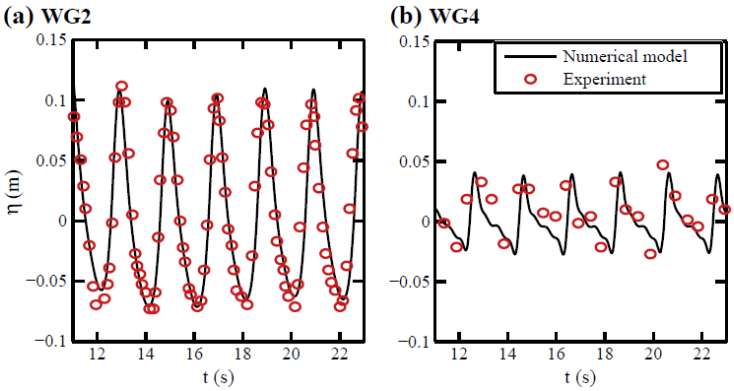

Fig. 2. Computed surface elevations (solid line) and measured surface elevations of Li et al. (2007) (circles) at (a) WG2 and (b) WG4.

the layer thickness at the crest of the structure. h_{meas} represents the landward ground level, positive for lower than structure crest and negative for higher than structure crest.

The average overtopping discharge rate is usually calculated by the ratio of accumulative overtopping volumes to the simulation time, or the overtopping velocity flux at $x=-B$ (Schüttrumpf and Oumeraci, 2005). However, the error in calculating overtopping volumes from VOF values (fraction of a computational cell filled with fluid) may accumulate and become significant in numerical modelling. For the case with the predicted average discharge of 0.67×10^{-3} m^3/s/m by TAW (2002), we found that the average discharge from VOF values during 300 s is 0.46×10^{-3} m^3/s/m, while the average discharge from the velocity flux is 0.61×10^{-3} m^3/s/m. Therefore, the product of layer thickness and overtopping velocity (velocity flux) is used to calculate the average overtopping discharge, $q_{t_0}(x=-\mathrm{B})$, from $t=0$ to $t=t_0$:

$$q_{t_0}=\frac{\int_0^{t_0}\sum_{y(j)=0}^{y(j_{max})}u_{i,j}(t)\Delta y_{i,j}dt}{t_0}\ at\ x(i)=-B \tag{1}$$

where $x(i)$,$u_{i,j}(t)$ and $\Delta y_{i,j}$ are the horizontal coordinate, horizontal velocity and cell height in the cell (i,j) respectively (Fig. 3). j_{max} is the maximum index of cells in the vertical direction and t_0 is the simulation time.

Table 1 lists a total of 22 tests with different wave conditions and coastal structural geometries used in this study. The outputs of each test

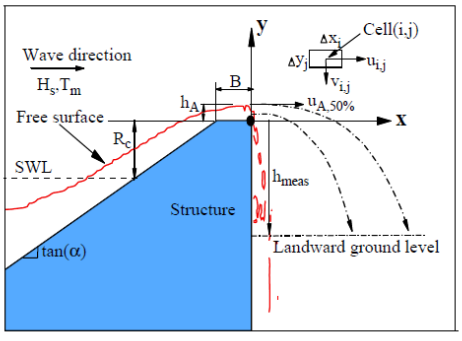

Fig. 3. Definitions of governing parameters involved in numerical simulations of wave overtopping.

case were sampled at 40 Hz for 300-second. 7 structure slopes, 4 relative crest widths, 8 landward ground levels and 3 relative freeboards are investigated. Random waves are generated through an internal wave-maker based on the TMA spectrum (Bouws et al., 1985). Fig. 4 shows that computed dimensionless overtopping discharges are in good agreements with Van der Meer and Janssen's empirical formulae and TAW formulae for a range of relative freeboard from 0.2 to 1.4. Computed overtopping discharge underestimated for relative freeboards larger than 1.2 because our model is not able to capture the overtopping volumes due to spray properly and air effect is ignored in the numerical model. de Waal et al. (1996) and Pullen et al. (2008) found that wind enhancement of overtopping is large when the discharge is small and the wind effect decreases as the discharge increases.

2.4. Spatial distribution of overtopping water behind the structure

Pullen et al (2008) and Lykke Andersen and Burcharth (2006) measured limited spatial distributions of wave overtopping water for a vertical wall and a sea dike with 1:2 seaward slope. Numerical simulations can provide high resolution results and are much more economical than physical experiments. The spatial distribution of wave overtopping water behind a structure is calculated by:

$$\frac{V(x)}{V_t}=\frac{\int_0^{t_0}\sum_{x(i)=x}^{x(i_{max})}v_{i,j}(t)\Delta x_{i,j}dt}{\int_0^{t_0}\sum_{x(i)=0}^{x(i_{max})}v_{i,j}(t)\Delta x_{i,j}dt}\ at\ y(j)=-h_{meas} \tag{2}$$

where $V(x)/V_t$ is the proportion of overtopping volume passing x at a specific landward ground level. $y(j)$, $v_{i,j}(t)$ and $\Delta x_{i,j}$ are the vertical coordinate, horizontal velocity and cell width in the cell (i,j) given by

Table 1
Overall view of test cases.

Parameters	Values
Test no.	22
H_s (significant wave height)	0.07 m–0.19 m
T_m (mean period)	1.0 s–2.0 s
Structure slope tan(α)	Vertical wall to 1:8
B/L_m (relative crest width)	0, 0.1, 0.2, 0.3
h_{meas} (landward ground level, cf. Fig. 3)	−0.05 m–0.3 m
R_c/H_s (relative freeboard)	0.32, 0.63 and 0.94

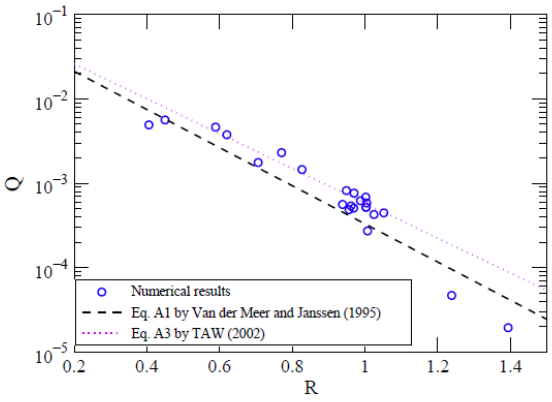

Fig. 4. Comparisons of dimensionless overtopping discharge, $Q=q_{to}/\sqrt{gH_s^3}$, against the dimensionless freeboards, $R=R_c/(H_s\xi_m)$ (ξ_m is surf similarity based on the mean period at the toe of structures), between model results and empirical formulae.

the RANS-VOF model (cf. Fig. 3). i_{max} is the maximum index of cells in the horizontal direction. t_0 is the simulation time and h_{meas} is the elevation where the distribution is measured (cf. Fig. 3).

As shown in Fig. 5, the proportion of overtopping volume passing a landward location x decays rapidly away from the structure. Therefore bulk of the overtopping water falls into the area immediately behind the structure. At zero landward ground level, model results agree reasonably well with the measurements, by Pullen et al (2008) for vertical wall with seven chambers (Fig. 5a) and Lykke Andersen and Burcharth (2006) for the slope of 1:2 with four chambers (Fig. 5b). Lykke Andersen's measurements are slightly underpredicted. This may be due to the overestimation of turbulence level near the breaking point by RANS-VOF model used in this study (Lin and Liu, 1998), which results in smaller wave energy to overtop due to extra energy dissipation. Therefore, a larger proportion of overtopping water falls into area close to coastal structures.

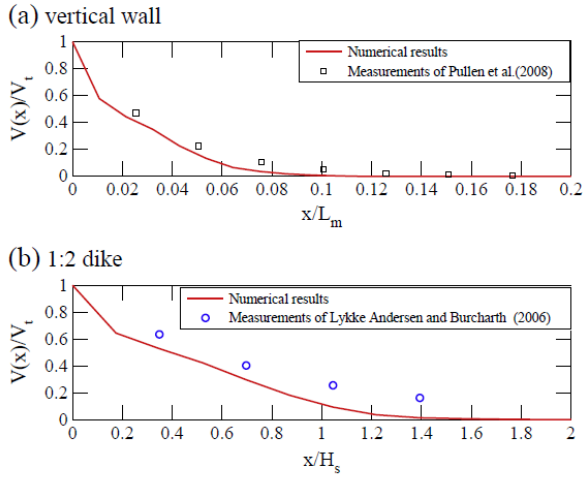

Fig. 5. Comparison of landward spatial distribution of overtopping water between model results and measurements for (a) a vertical wall and (b) a sea dike with the seaward slope of 1:2. $V(x)/V_t$ is the proportion of overtopping volume passing a landward location x; V_t is the total overtopping volume; L_m indicates wave length with the mean period and H_s is significant wave height at the toe of sea dike; landward ground level $h_{meas}=0$ m for both cases.

3. Semi-analytical model

It is well known that wave run-up significantly affects the wave overtopping process. For a given freeboard of coastal structure, wave overtopping increases with wave run-up. Hunt (1959) proposed the following formula for the 2% relative run-up level on impermeable structures:

$$\frac{R_{u2\%}}{H_s}=c_1\xi_m \quad \xi_m\le\xi_{cr} \tag{3}$$

$$\frac{R_{u2\%}}{H_s}=c_1\xi_{cr}=2c_1 \quad \xi_m>\xi_{cr} \tag{4}$$

where $c_1=1.5$ for irregular wave and 1.0 for regular wave; H_s is the significant wave height at the toe of the dike and T_m the mean wave period; $L_m=gT_m^2/(2\pi)$ the deep water wave length; ξ_m the surf similarity: $\xi_m=tan(\alpha)/\sqrt{H_s/L_m}$; ξ_{cr} the surf similarity at transition point between plunging and surging breakers; $R_{u2\%}$ is the run-up that only 2% of the wave run-up values observed will reach or exceed.

It is expected that spatial distribution of wave overtopping water behind the structure is mainly affected by the landward ground level, the horizontal velocity and the layer thickness on the landward end of the dike crest. Schüttrumpf and Oumeraci (2005) derived formulae of layer thickness on the landward end of the crest ($x=0$):

$$\begin{aligned} h_A&=c_2x_Z\left(1-\frac{R_c}{\tan(\alpha)x_Z}\right)\exp(-c_3)\\ x_Z&=c_1\sqrt{H_sL_m} \quad \xi_m\le\xi_{cr}\\ x_Z&=c_1\frac{2.0H_s}{\tan\alpha} \quad \xi_m>\xi_{cr}\end{aligned} \tag{5}$$

where h_A is the layer thickness on the landward end of the crest; x_Z the horizontal wave run-up length; $\tan(\alpha)$ the structure slope; $c_2=0.168/\tan\alpha$, $c_3=0.75$ (for irregular wave); g the gravity acceleration.

Schüttrumpf and Oumeraci (2005) found that the variation of the overtopping velocity along the dike crest width is influenced by bottom friction. The dike crest employed here is relatively short ($B=0.30$ m) and assumed hydraulically smooth. Therefore, the velocity changes along the dike crest can be ignored. The horizontal velocity at the landward end of the crest ($x=0$ m) $u_{A,50\%}$, which is exceeded by 50% of the incoming waves, is usually used to describe the fluid velocity on the structure crest by previous researchers, such as Schüttrumpf and Oumeraci (2005); Bosman et al. (2008) and this velocity is convenient to be used due to its relationship with the wave run-up. Therefore, $u_{A,50\%}$ can be calculated as (Schüttrumpf and Oumeraci, 2005):

$$u_{A,50\%}=0.94\sqrt{gH_s}\sqrt{\frac{R_{u2\%}}{H_s}-\frac{R_c}{H_s}} \tag{6}$$

Following the Newton's Second Law of Motion, the landward trajectory of overtopping water with initial velocity, $u_{A,50\%}$, takes the shape of a parabola. The travel distance x of the overtopping water at an elevation above the crest, y_c, is given by:

$$x(y_c)=u_{A,50\%}\sqrt{\frac{2(y_c+h_{meas})}{g-a_{ay}}}+\left(\frac{\partial u_{A,50\%}}{\partial t}-a_{ax}\right)\frac{y_c+h_{meas}}{\left(g-a_{ay}\right)}\,0\le y_c\le h_A \tag{7}$$

where a_{ax} and a_{ay} represent the acceleration induced by the air resistance.

By assuming that the air effect is negligible and the horizontal acceleration of the overtopping water is zero, Eq. (7) can be rewritten in a simpler form:

$$x(y_c)=u_{A,50\%}\sqrt{\frac{2(y_c+h_{meas})}{g}} \quad 0\le y_c\le h_A \tag{8}$$

By dividing the layer thickness, h_A, into segments with the same thickness, the proportion of overtopping volume passing landward location x can be calculated from Eqs. (5)–(8).

A case of irregular wave overtopping over a 1:6 sea dike was investigated, with $H_s = 0.12$ m, $T_m = 1.6$ s and the same geometry as shown in Fig. 1. Fig. 6 shows the comparisons of landward spatial distribution of the overtopping water predicted by the semi-analytical and the numerical model and measurements. The semi-analytical model is in good agreement with the numerical model close to a 1:6 dike where there is a large proportion of overtopping water. The discrepancy only takes up a small proportion of overtopping water at locations far away from structures (Fig. 6a). The semi-analytical prediction of spatial distribution of overtopping water over a 1:2 dike agrees reasonably well with both numerical model results and measurements close to the structure (Fig. 6b). However, numerical model results and measurements tend to spread the overtopping water into a broader area, close to structures or far away from structures for both cases. Since the semi-analytical model used a velocity on the structure crest which 50% of the incoming waves will exceed, waves with velocities smaller or larger than this velocity result in overtopping water to travel closer or farther. Significant wave height used in Eqs. (5) and (6), H_s, is approximately the average height of one-third largest waves; therefore, the semi-analytical model ignores the overtopping contributions of some individual smaller or larger waves, which are able to travel closer or farther.

Analytical and semi-analytical models have been popular for their tractability to validate experimental data and model results. Results above show that semi-analytical model is able to estimate the spatial distribution of overtopping water close to coastal structures, where there is large proportion of overtopping water. The semi-analytical model, thus, provides an easy tool for engineers to predict the spatial distribution of wave overtopping water behind breakwaters. This model can offer a general concept of spatial distribution of overtopping water and would give an idea of the ranges of hazard zones expected in a specific setup. Numerical model is next used to analyze the controlling factors of spatial distribution of wave overtopping to complement the semi-analytical model.

4. Parameter analysis of numerical model results

We will next look at the effect of structure slope, $\tan(\alpha)$, significant wave height, H_s, mean period, T_m, relative structure crest width, B/L_m, relative structure freeboard, R_c/H_s and landward ground level, h_{meas}, on the landward distribution of the overtopping water over coastal structures. These parameters were found to be important in wave overtopping process over coastal structures in the semi-analytical model.

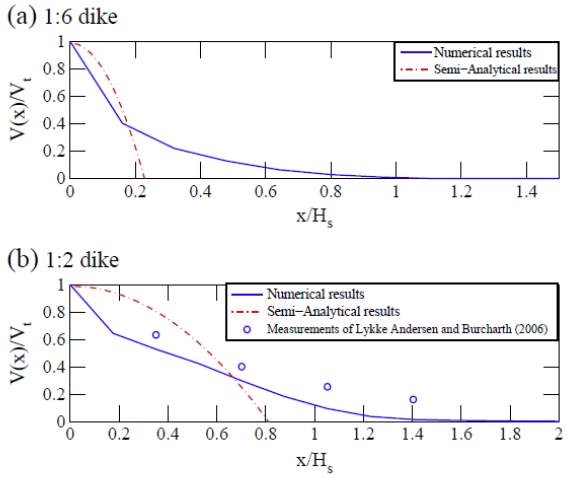

Fig. 6. Comparisons of landward spatial distribution of overtopping water over (a) a 1:6 dike and (b) a 1:2 dike between semi-analytical model, numerical model and experiments. $H_s = 0.12$ m, $T_m = 1.6$ s, $h = 0.7$ m, $\tan(\alpha) = 1{:}6$, $R_c = 0.1$ m and $h_{meas} = 0$ m.

4.1. Structure slope

Different types of breaking waves, such as spilling, plunging, collapsing and surging, may occur on the coast depending on the surf similarity, consisting of incident wave steepness and bottom slope (Battjes, 1974). Wave energy reflected from the coast is also dependent on the surf similarity. Therefore, seaward slopes affect wave reflection coefficients, wave breaker types and wave run-ups. Seven structure slopes of 1:8, 1:6, 1:4, 1:3, 1:2, 1:1 and a vertical wall are examined.

As shown in the Fig. 7, the proportion of wave overtopping volume passing x increases as the structure slope increases from 1:8 to 1:3, but it decreases as the slope increases further from 1:3 to a vertical wall. All the proportion of wave overtopping water decreases exponentially with distance x away from the structure. The effect of seaward slopes on spatial distribution of overtopping water is not monotonic. This can be explained as following: For milder slope, wave breaker is likely to be a spilling or plunging breaker and wave reflection coefficient is small. Wave loses more energy to breaking and has less wave energy reflected. Eqs. (3)–(8) also show that for breaking waves, the steeper slope leads to the larger wave run-up and extent of hazard area. Over a steeper slope, the wave tends not to break, or has a surging breaker; wave reflection coefficient is large, and standing waves may also be formed. Therefore, wave energy is mainly reflected and has less wave energy dissipated due to wave breaking. This is consistent with the findings by Sunamura and Okazaki (1996) that the reflection coefficient increases as the breaker type changes from spilling to collapsing through plunging, as the structure slope increases. Both wave breaking and reflection on the seaward slopes decrease the horizontal velocity and layer thickness on the crest, which are the key parameters for the landward spatial distribution shown in Eq. (8). For example, the slope of 1:8 has more breaking induced energy loss than the slope of 1:1 but less wave energy reflected from the structure, therefore, the combination effect of wave breaking and reflection leads to maximum overtopping for the slope between 1:8 and 1:1.

4.2. Relative structure freeboard

The structure freeboard relative to significant wave height at the toe of structures, R_c/H_s, is significant to the velocity and layer thickness

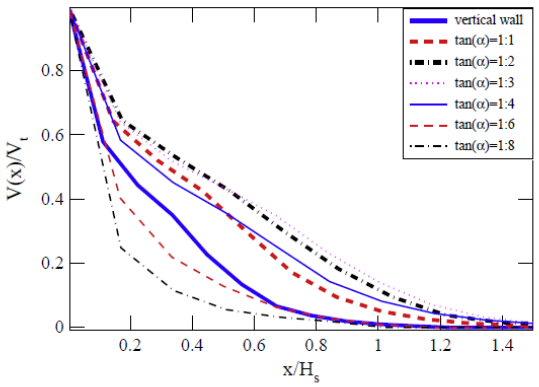

Fig. 7. Effect of structure seaward slopes, $\tan(\alpha)$, on landward spatial distribution of wave overtopping water. $H_s = 0.12$ m, $T_m = 1.6$ s, $h = 0.7$ m, $h_{meas} = 0$ m, $R_c = 0.1$ m and $B = 0.3$ m.

on the structure crest, according to Eqs. (5) and (6). Fig. 8 shows that relative structure freeboards have significant effect on landward spatial distribution of wave overtopping water. For a certain landward location, the proportion of wave overtopping volume passing x decreases with increasing relative structure freeboards. For example, the majority of overtopping water travels about one significant wave height away from structures for relative freeboard of 0.94, but it travels farther behind structures, up to 1.6 times the significant wave height for a relative freeboard of 0.32. This is mainly due to the change in horizontal velocity on the crown crest. Due to the gravity effect, large relative freeboard requires more potential energy to overtop the crest; therefore, the kinetic energy will decrease. Small kinetic energy corresponds to small horizontal velocity on the crown crest. Therefore, large relative freeboard leads to small travel distance of overtopping water.

4.3. Landward ground level

It can be expected that the spatial distribution of the overtopping water depends on the landward ground level, h_{meas}. As discussed in the Section 3, the trajectory of overtopping volume is in a parabolic type, therefore, we can estimate that if the overtopping volume is dropped into $x = \sqrt{\frac{2(y+0)}{g}}$ m at $h_{meas} = 0$ m, then it will fall into $x = \sqrt{\frac{2(y+0.1)}{g}}$ at $h_{meas} = 0.1$ m instead. Fig. 9 shows the effect of landward ground level on landward spatial distribution of overtopping water as a function of relative landward distance. The positive h_{meas} stands for the ground level lower than the structure crest and negative h_{meas} represents the ground level higher than the structure crest.

It is interesting to observe that for the same wave conditions and structural geometry the proportion of wave overtopping volume passing x increases with landward ground level, h_{meas}. The overtopping water even reaches to a distance up to three times bigger than significant wave height for $h_{meas} = 0.2$ m, while it only splashes down in the area of half the significant wave height from structures for $h_{meas} = -0.05$ m. However, the computed proportion of wave overtopping water passing a landward location is smaller than predictions by Eq. (6.17) in EurOtop (2008), in accord with more overtopping water falling into the area just behind the structure. This is mainly due to a nappe (in hydro-engineering refers to the sheet of water over-topping) clinging to the landward face of the weir with very low water heads.

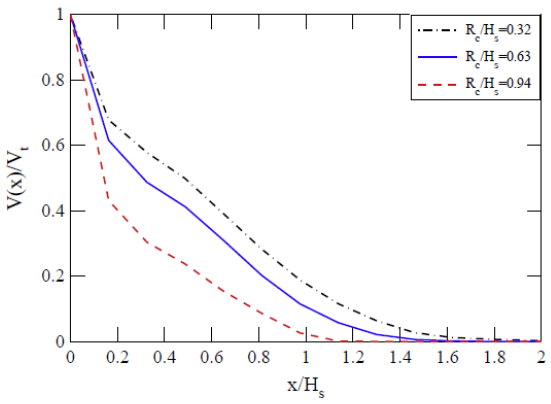

Fig. 8. Effect of relative structure freeboards on landward spatial distribution of overtopping water. $H_s = 0.16$ m, $T_m = 2.0$ s, $h = 0.7$ m, $h_{meas} = 0$ m, $B = 0.3$ m and $\tan(\alpha) = 1{:}6$.

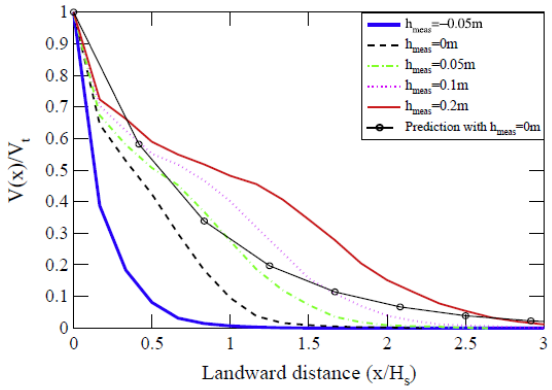

Fig. 9. Effect of landward ground level, h_{meas}, on computed landward spatial distribution of overtopping water. Prediction is given by Eq. (6.17) in EurOtop (2008) with $h_{meas} = 0$. The positive h_{meas} stands for the ground level lower than the structure crest. $H_s = 0.12$ m, $T_m = 1.6$ s, $h = 0.7$ m, $R_c = 0.1$ m, $\tan(\alpha) = 1{:}2$ and $B = 0.3$ m.

4.4. Structure porosity

Structure porosity will affect spatial distribution of overtopping water through wave run-up and velocities on the crest as suggested by Eq. (8). In this study, four types of coastal structures have been employed and shown in Fig. 10, including a caisson breakwater with concrete protection; caisson breakwater with gravel protection (porosity $n = 0.49$); caisson breakwater with rubble protection (porosity $n = 0.53$) and rubble mound breakwater. The present model investigates the porous media in a similar way as Liu et al. (1999) by averaging the flow equations over a length scale. This length scale is larger than the characteristic pore size and is much smaller than the scale of the spatial variation of the physical variables in the flow domain. Therefore, the fluid variables can be decomposed into two parts, spatially averaged and spatially fluctuated quantities.

Fig. 11 shows the spatial distribution of wave overtopping water for various structure porosity at the ground level $h_{meas} = 0$ m. With the same incident wave conditions ($H_s = 0.12$ m, $T_p = 1.6$ s) and the same geometry, the proportion of wave overtopping volume passing x decreases with structure porosity. This is because the employment of permeable protection leads to effective energy dissipation and reduces the overtopping discharge (Liu et al., 1999). In addition, large porosity, equivalent to large roughness or surface friction, leads to large dissipation and deductions of velocity and layer thickness on the structure crest. The proportion of wave overtopping volume passing a landward location for rubble mound breakwater is significantly smaller than that for caisson breakwater with rubble protection (Fig. 11). The structure crest is hydraulically rough for the former case but hydraulically smooth for the latter, although these two layouts have the same structure porosity. Therefore, rubble mound breakwater has smaller velocity of the overtopping water on the crest. As can be seen in Eq. (8), small velocity and layer thickness result in small travel distance of the overtopping water. This finding is consistent with the recommendation by EurOtop (2008) that roughness elements located above the still water level minus a quarter of wave run-up on a smooth slope, has a significant effect on the wave overtopping discharge.

4.5. Incident wave condition

It is well known that both wave height and wavelength are very important to the wave overtopping discharge (Eq. (A1)–(A4)). Semi-analytical model shows that layer thickness, h_A, is proportional to horizontal run-up length, x_z, in Eq. (5) and wave run-up velocity, $u_{A,50\%}$,

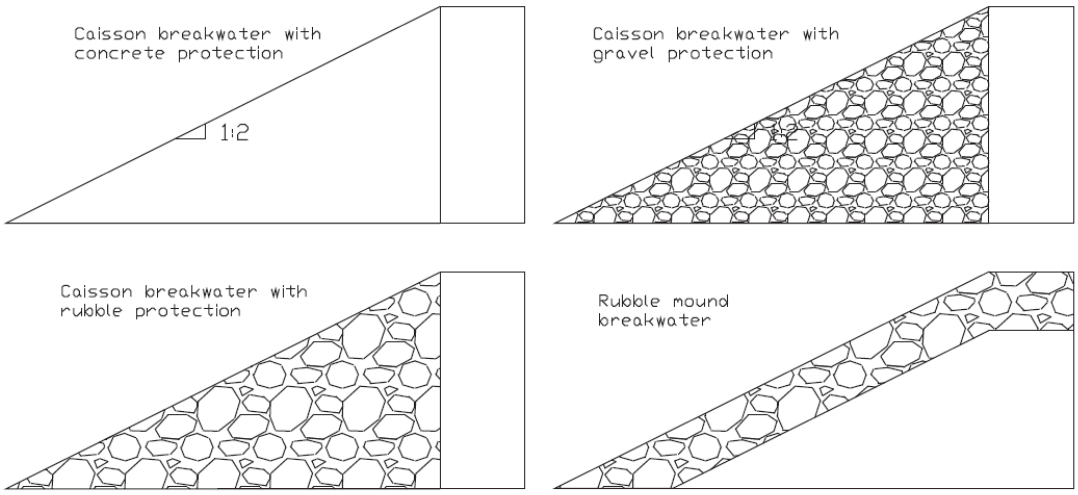

Fig. 10. Layouts of four different coastal structures.

is related to wave run-up, $R_{u2\%}$, in Eq. (6). Therefore, both h_A and $u_{A,50\%}$ are related to the square root of the product of wave height and wavelength, $\sqrt{H_s L_m}$. As can be found from Eq. (8), we can conclude that $\sqrt{H_s L_m}$ is a key parameter controlling the spatial distribution of overtopping water. Given water depth of 0.7 m and structural geometry, four cases with different incident wave heights and mean wavelengths, $\sqrt{H_s L_m}$ have been used to investigate the effect of incident wave conditions.

Fig. 12a shows the effect of incident wave conditions on landward spatial distribution of wave overtopping water. At the same relative landward distance, the proportion of overtopping water passing x increases with $\sqrt{H_s L_m}$. For a small $\sqrt{H_s L_m}$, a large part of the overtopping water falls into the locations close to the structure, but for a large $\sqrt{H_s L_m}$ it falls into the area farther away from the structure. It is shown in Fig. 12a that the overtopping water mainly falls within one-quarter of the significant wave height behind the structure for $\sqrt{H_s L_m} = 0.46$ m, while it falls into a larger area, up to one and half significant wave heights behind the structure for $\sqrt{H_s L_m} = 0.65$ m.

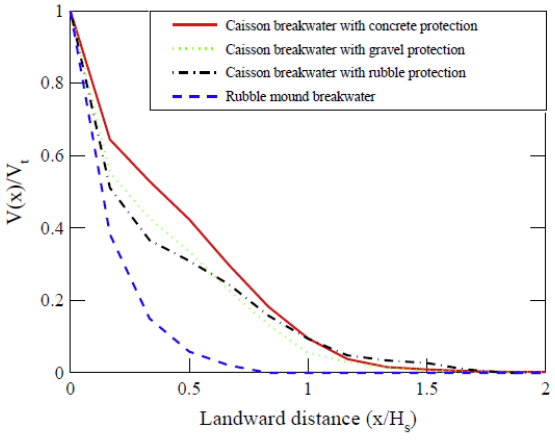

Fig. 11. Effect of structure porosity on landward spatial distribution of wave overtopping water. $H_s = 0.12$ m, $T_m = 1.6$ s, $h = 0.7$ m, $h_{meas} = 0$ m, $R_c = 0.1$ m and $B = 0.3$ m.

4.6. Relative structure crest width

The relative crest width, defined as the ratio of the crest width, B, to the deep water mean wavelength, L_m, is significant to the layer thickness and velocity on the structure crest (Schüttrumpf and Oumeraci, 2005). Therefore, it can be expected that the landward spatial distribution of overtopping water is dependent on the relative crest width based on semi-analytical model.

Fig. 12b shows the spatial distribution of wave overtopping water against relative landward distance, x/H_s. Given incident wave conditions ($H_s = 0.12$ m, $T_m = 1.6$ s) and structural geometry, the proportion of wave overtopping volume passing x increases significantly as the relative crest width decreases from 0.3 to 0. This is because large relative crest width leads to large deductions of velocity and layer thickness on the structure crest due to the friction and the deformation of the overtopping tongue on the structure crest respectively (Schüttrumpf and Oumeraci, 2005; Bosman et al., 2008). Therefore, for the same velocity and layer thickness on the seaward end of structure crest ($x = -$B), larger relative crest width corresponds to a smaller velocity and layer thickness on the landward end of structure crest ($x = 0$ m). Based on Eq. (8), small velocity and layer thickness result in small travel distance of the overtopping water.

4.7. Overtopping discharge per wave and its distribution

Fig. 13a shows the overtopping discharge variation with time. The maximum individual overtopping discharge is 0.014 $m^3/m/s$ at 10th wave cycle and the overall time average overtopping discharge is around 0.0025 $m^3/m/s$ for 160 waves. Fig. 13b shows the spatial distribution of overtopping water behind coastal structures for the 160 wave cycles. Overtopping water decays exponentially with landward distance, this result is similar to the previous experimental results by Jensen and Sorensen (1979), Bruce et al. (2005), Lykke Andersen and Burcharth (2006) and Pullen et al. (2008). The distribution of maximum overtopping event has a similar trend to the time average distribution and the former is larger than the latter by a magnitude of 0.2 approximately. Fig. 13b also shows that extent of hazard zone due to wave overtopping increases with overtopping discharge. This is mainly because wave overtopping discharge approximately equals the product of velocity and thickness on the structure crest, which affects spatial distribution of overtopping water. The relationship of spatial distribution of overtopping water

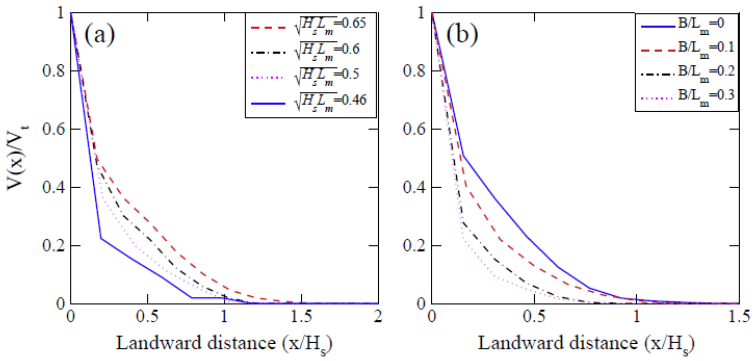

Fig. 12. Effect of (a) incident wave conditions, $\sqrt{H_s L_m}$, and (b) relative structure crest width, B/L_m, on landward spatial distribution of overtopping water over a coastal structure.

between maximum overtopping event and time average distribution behind coastal structures remains to be studied in the future.

5. Conclusions

Spatial distribution of random wave overtopping water behind coastal structures was investigated using a RANS-VOF model and a semi-analytical model. Computed overtopping discharges agree well with van der Meer and Janssen (1995) and TAW (2002) based on physical models and empirical formulae. Computed landward spatial distributions of wave overtopping water are in good agreement with the measurements by Pullen et al (2008) for a vertical seawall and Lykke Andersen and Burcharth (2006) for a 1:2 dike. The proportion of wave overtopping water passing a landward location decreases exponentially with the landward distance, corresponding to the bulk of wave overtopping water falling into areas immediately behind the structure. Our model results suggest that the proportion of wave overtopping water passing a landward location increases with the seaward slope from 1:8 to 1:3, but it decreases with the seaward slope from 1:3 to 1:0 for a vertical wall. The proportion of wave overtopping water passing a landward location increases with landward ground level (cf. h_{meas} in Fig. 3) and overtopping discharge. It also increases with the product of incident wave height and wavelength, but decreases with relative structure freeboard and crest width. The extent of hazard area due to wave overtopping is significantly reduced by using a permeable structure crown.

We derived a semi-analytical model relating the landward spatial distribution of wave overtopping water to the landward ground level, the velocity and layer thickness on the crest. This model agrees reasonably well with both numerical model results and measurements close to coastal structures where majority overtopping water is. This model can be combined with the empirical formulae of velocity and layer thickness on the structure crest by Schüttrumpf and Oumeraci (2005) to estimate the extent of overtopping water without resorting to numerical modelling.

Our study suggests that in practical application, by adopting structure slopes smaller than 1:3, large relative crest widths and freeboards, permeable structure crown, as well as locating properties behind coastal defences at a small ground level (positive downward, cf. h_{meas} in Fig. 3), we may reduce the hazard area due to wave overtopping behind the defence. However, more comprehensive measurements of wave overtopping distribution are needed to enhance our understanding of this problem. The transformation of wave asymmetries over coastal structures, studied by Peng et al. (2009) and Zou and Peng (2011), may also affect the landward spatial distribution of the overtopping water.

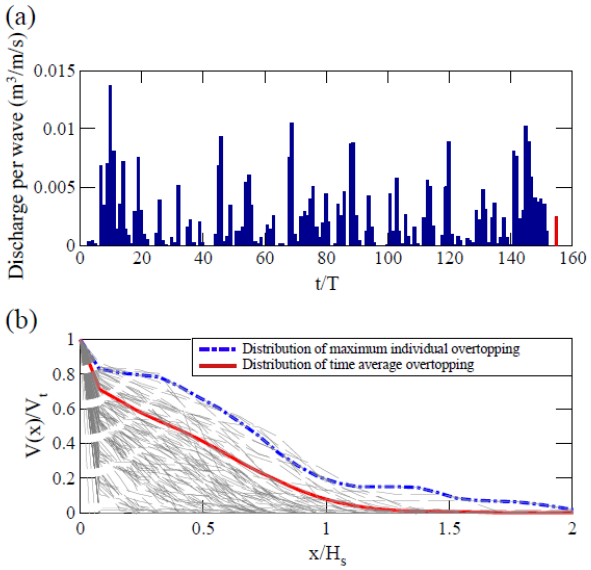

Fig. 13. (a) Overtopping discharge per wave cycle (red bar: overall time average overtopping discharge) and (b) landward spatial distribution of the overtopping water over a 1:2 dike. Thin dashed lines: spatial distribution of overtopping water for individual wave cycles.

List of symbols

B	Crest width (m)
h_{toe}	Water depth at the toe of coastal structures (m)
h_{meas}	Landward ground level with $h_{meas}=0$ at structure crest level. Positive for lower than structure crest and negative for higher than structure crest (m)
H_s	Significant wave height at the toe of coastal structures (m)
T_m	Mean wave period at the toe of coastal structures (s)
L_m	Deep water mean wavelength, $L_m=gT_m^2/(2\pi)$ (m)
n	Structure porosity (−)
q_{t0}	Average overtopping discharge between $t=0$ and $t=t_0$ (m³/s/m)
Q	Dimensionless overtopping discharge, $Q=q_{t_0}/\sqrt{g*H_s^3}$ (−)
R_c	Structure freeboard (m)
R	Dimensionless structure freeboards, $R=R_c/(H_s\xi_p)$ (−)

S_0	Mean wave steepness, $S_0 = H_s/L_m$ (−)
$\tan(\alpha)$	Seaward slope of coastal structures (−)
U_r	Ursell number, $U_r = H_s L_m^2/h^3$ (−)
V_t	Accumulative overtopping volume at t (m^3/ m)
$V(x)/V_t$	Proportion of average overtopping water passing a location x (−)
ξ_m	Surf similarity, $\xi_m = \tan(\alpha)/(S_0)^{0.5}$ (−)
ξ_p	Surf similarity, $\xi_p = \tan(\alpha)/(S_{op})^{0.5}$ (−)
η	Wave surface elevation (m)
γ_f	Roughness (m)
h_A	Layer thickness on the landward end of structure crest (m)
$u_{A,50\%}$	Velocity on the structure crest which 50% incident wave will exceed (m/s)
y_c	Elevation above the crest
$u_{i,j}$	Horizontal velocity in the cell (i, j) (m/s)
$v_{i,j}$	Vertical velocity in the cell (i, j) (m/s)
$dx_{i,j}$	Cell width in the cell (i, j) (m)
$dy_{i,j}$	Cell height in the cell (i, j) (m)

Acknowledgements

The authors would like to thank Professor Pengzhi Lin at State Key Laboratory of Hydraulics and Mountain River Engineering in Sichuan University, who generously supplied his RANS-VOF code for the present work, along with the support of the Natural Environmental Research Council (Grant No. NE/E002129/1). This work was carried out while Zhong Peng was in receipt of a University of Plymouth postgraduate research scholarship.

Appendix A. Design formulae of overtopping discharge

A combination of storm surge and large waves may cause overtopping of such structures like breakwaters, dikes, seawalls, etc., leading to damage to and flooding of the area behind the structure. Overtopping is defined as the water volume passing over the crest of structures per unit length in a unit time. The average discharge q has the unit of $m^3/m/s$.

A.1. Van der Meer and Janssen formula

The common used formula for calculating wave overtopping rates is derived by van der Meer and Janssen (1995) from experimental data.

For breaking waves (plunging): $\xi_p < 2$

$$\frac{q}{\sqrt{g*H_5^3}} = \frac{0.06}{\sqrt{\tan\alpha}} * \xi_p * \exp\left(-5.2 * \frac{R_c}{\xi_p * H_s * \gamma_r * \gamma_b * \gamma_h * \gamma_\beta}\right) \quad (A1)$$

For non-breaking waves (surging): $\xi_p > 2$

$$\frac{q}{\sqrt{g*H_5^3}} = 0.2 * \exp\left(-2.6 * \frac{R_c}{H_s * \gamma_r * \gamma_b * \gamma_h * \gamma_\beta}\right) \quad (A2)$$

Where α is the slope of the front face of the structure, R_c is the structure freeboard, H_s significant wave height ($= H_{1/3}$) at the toe of the slope and L_{op} being the deep water wave length $gT_p^2/(2\pi)$. $\xi_p = \frac{\tan\alpha}{\sqrt{H_s/L_{op}}}$. The coefficients γ_b, γ_h, γ_r, and γ_β are introduced to take into account the influence of a berm, shallow foreshore, roughness and oblique wave attach. All these coefficients are equal to 1.0 in present work.

A.2. TAW (2002) formula

EurOtop Manual (EurOtop, 2008) recommends the formulae to probability design and prediction proposed by TAW (2002) for breaking and non-breaking waves ($\xi_{m-1,0} < 5$):

$$\frac{q}{\sqrt{g*H_{m0}^3}} = \frac{0.067}{\sqrt{\tan\alpha}} * \gamma_b * \xi_{m-1,0} * \exp\left(-4.75 * \frac{R_c}{\xi_{m-1,0} * H_{m0} * \gamma_f * \gamma_\beta}\right) \quad (A3)$$

With a maximum of: $\frac{q}{\sqrt{g*H_{m0}^3}} = 0.2 * \exp\left(-2.6 * \frac{R_c}{H_{m0} * \gamma_f * \gamma_\beta}\right)$.

The formulae to deterministic design and prediction:

$$\frac{q}{\sqrt{g*H_{m0}^3}} = \frac{0.067}{\sqrt{\tan\alpha}} * \gamma_b \xi_{m-1,0} * \exp\left(-4.3 * \frac{R_c}{\xi_{m-1,0} * H_{m0} * \gamma_b * \gamma_f * \gamma_\beta * \gamma_v}\right) \quad (A4)$$

With a maximum of: $\frac{q}{\sqrt{g*H_{m0}^3}} = 0.2 * \exp\left(-2.3 * \frac{R_c}{H_{m0} * \gamma_f * \gamma_\beta}\right)$.

Where α is the slope of the front face of the structure, R_c is the structure freeboard, H_{m0} is the energy spectrum based significant wave height at the toe of the slope and $T_{m-1,0}$ being the mean energy wave period, $L_{m-1,0} = gT^2_{m-1,0}/(2\pi)$. $\xi_{m-1,0} = \frac{\tan\alpha}{\sqrt{H_{m0}/L_{m-1,0}}}$. The coefficients γ_b, γ_f, γ_β, and γ_v are introduced to take into account the influence of a berm, permeability and roughness of or on the slope, oblique wave attach and a vertical wall on the slope respectively. All these coefficients are equal to 1.0 in present work.

References

Allsop, W., Bruce, T., Pearson, J., Besley, P., 2005. Wave overtopping at vertical and steep seawalls. Proceedings of the ICE - Water Maritime and Energy 158 (3), 103–114.

Battjes, J.A., 1974. Surf similarity, Proceedings of 14th International Conference on Coastal Engineering. American Society of Civil Engineers, Copenhagen, Denmark, pp. 466–480.

Bosman, G., Meer, J.v.d., Hoffmans, G., Schüttrumpf, H., Verhagen, H.J., 2008. Individual overtopping events at dikes. Proceedings of the 31st International Conference on Coastal Engineering, Hamburg, Germany, pp. 2944–2956.

Bouws, E., Günther, H., Rosenthal, W., Vincent, C.L., 1985. Similarity of the Wind Wave Spectrum in Finite Depth Water 1. Spectral Form. J. Geophys. Res. 90 (C1), 975–986.

Bruce, T., Pullen, T., Allsop, N.W.H., Pearson, J., 2005. How far back is safe? Spatial distributions of wave overtopping. Telford, London, Proceedings of the Coastlines, Seawalls and Breakwaters, ICE. Thomas Telford, London.

Bruce, T., van der Meer, J.W., Franco, L., Pearson, J.M., 2009. Overtopping performance of different armour units for rubble mound breakwaters. Coastal Eng. 56 (2), 166–179.

de Waal, J.P., Tönjes, P., Van der Meer, J.M., 1996. Overtopping of sea defences. In: Edge, B.L. (Ed.), Proceedings of the 25th International Conference on Coastal Engineering. ASCE, Orlando, Florida, USA, pp. 2216–2229.

EurOtop, 2008. In: Pullen, T., Allsop, N.W.H., Bruce, T., Kortenhaus, A., Schuttrumpf, H., Van der Meer, J. (Eds.), Wave Overtopping of Sea Defences and Related Structures – Assessment Manual. http://www.overtopping-manual.com.

Garcia, N., Lara, J.L., Losada, I.J., 2004. 2-D numerical analysis of near-field flow at low-crested permeable breakwaters. Coastal Eng. 51 (10), 991–1020.

Hirt, C.W., Nichols, B.D., 1981. Volume of fluid (VOF) method for the dynamics of free boundaries. J. Comput. Phys. 39 (1), 201–225.

Hu, K., Mingham, C.G., Causon, D.M., 2000. Numerical simulation of wave overtopping of coastal structures using the non-linear shallow water equations. Coastal Eng. 41 (4), 433–465.

Hughes, S.A., Nadal, N.C., 2009. Laboratory study of combined wave overtopping and storm surge overflow of a levee. Coastal Eng. 56 (3), 244–259.

Hunt, A.C., 1959. Design of seawalls and breakwaters. Journal of Waterway and Harbour division 85 (3), 123–152.

Ingram, D.M., Gao, F., Causon, D.M., Mingham, C.G., Troch, P., 2009. Numerical investigations of wave overtopping at coastal structures. Coastal Eng. 56 (2), 190–202.

Jensen, O.J., Sorensen, T., 1979. Overspilling/overtopping of rubble-mound breakwaters. Results of studies, useful in design procedures. Coastal Eng. 3, 51–65.

Lara, J.L., Garcia, N., Losada, I.J., 2006. RANS modelling applied to random wave interaction with submerged permeable structures. Coastal Eng. 53 (5–6), 395–417.

Li, T., Troch, P., De Rouck, J., 2004. Wave overtopping over a sea dike. J. Comput. Phys. 198 (2), 686–726.

Li, T., Troch, P., Rouck, J.D., 2007. Interactions of breaking waves with a current over cut cells. J. Comput. Phys. 223 (2), 865–897.
Lin, P.Z., Liu, P.L.F., 1998. A numerical study of breaking waves in the surf zone. J. Fluid Mech. 359, 239–264.
Lin, P.Z., Liu, P.L.F., 1999. Internal wave-maker for Navier-Stokes equations models. Journal of Waterway Port Coastal and Ocean Engineering 125 (4), 207–215.
Liu, P.L.F., Lin, P.Z., Chang, K.A., Sakakiyama, T., 1999. Numerical modeling of wave interaction with porous structures. J. Waterw. Port Coast. Ocean Eng. 125 (6), 322–330.
Losada, I.J., Lara, J.L., Guanche, R., Gonzalez-Ondina, J.M., 2008. Numerical analysis of wave overtopping of rubble mound breakwaters. Coastal Eng. 55 (1), 47–62.
Lykke Andersen, T., Burcharth, H.F., 2006. Landward distribution of wave overtopping for rubble mound breakwaters. Proceedings of the First International Conferece on the Application of Physical Modelling to Port and Coastal Protection. IAHR, Porto, Portugal, pp. 401–411.
Lykke Andersen, T., Burcharth, H.F., 2009. Three-dimensional investigations of wave overtopping on rubble mound structures. Coastal Eng. 56 (2), 180–189.
Lykke Andersen, T., Burcharth, H.F., Gironella, F.X., 2007. Single wave overtopping volumes and their travel distance for rubble mound breakwaters. The 5th International Conference on Coastal Structures, Venice, Italy.
Owen, M.W., 1980. Design of sea walls allowing for wave overtopping, Report EX. 924. Hydraulics Research Station, Wallingford, UK.
Peng, Z., Zou, Q.-P., Reeve, D.E., Wang, B.X., 2009. Parameterisation and transformation of wave asymmetries over a low-crested breakwater. Coastal Eng. 56 (11–12), 1123–1132.
Pullen, T., Allsop, W., Bruce, T., Pearson, J., 2008. Field and laboratory measurements of mean overtopping discharges and spatial distributions at vertical seawalls. Coastal Eng. 56 (2), 121–140.
Reeve, D.E., Soliman, A., Lin, P.Z., 2008. Numerical study of combined overflow and wave overtopping over a smooth impermeable seawall. Coastal Eng. 55 (2), 155–166.
Rodi, W., 1993. Turbulence models and their application in hydraulics – a state of the art review. IAHR Monografia, Delft.
Schüttrumpf, H., Oumeraci, H., 2005. Layer thicknesses and velocities of wave overtopping flow at seadikes. Coastal Eng. 52 (6), 473–495.
Shao, S.D., Ji, C., Graham, D.I., Reeve, D.E., James, P.W., Chadwick, A.J., 2006. Simulation of wave overtopping by an incompressible SPH model. Coastal Eng. 53 (9), 723–735.
Sunamura, T., Okazaki, S.-i., 1996. Breaker types and wave reflection coefficient: laboratory relationships. J. Coast. Res. 12 (1), 240–245.
TAW, 2002. Technical report on wave run-up and wave overtopping at dikes. In: Meer, J.W.v.d. (Ed.), Technical Advisory Committee for Flood Defence, The Netherlands. http://www.tawinfo.nl.
Troch, P., Geeraerts, J., Van de Walle, B., De Rouck, J., Van Damme, L., Allsop, W., Franco, L., 2004. Full-scale wave-overtopping measurements on the Zeebrugge rubble mound breakwater. Coastal Eng. 51 (7), 609–628.
van der Meer, J., Janssen, J.P.F.M., 1995. Wave run-up and wave overtopping at dikes. In: Kobayashi, N., Demirbilek, Z. (Eds.), Wave forces on inclined and vertical structures. ASCE, pp. 1–27.
van der Meer, J.W., Verhaeghe, H., Steendam, G.J., 2009. The new wave overtopping database for coastal structures. Coastal Eng. 56 (2), 108–120.
Xiao, H., Huang, W., Tao, J., 2009. Numerical modeling of wave overtopping a levee during Hurricane Katrina. Comput. Fluids 38 (5), 991–996.
Zou, Q.-P., Peng, Z., 2011. Evolution of wave shape over a Low-crested Structure. Coastal Eng. doi:10.1016/j.coastaleng.2011.01.00.